GEOFIZIKA VOL. 29 2012

Original scientific paper
UDC 551.551.2

Large scale turbulence structures in the Ekman boundary layer

Igor Esau

Nansen Environmental and Remote Sensing Centre, G. C. Rieber Climate Institute, Bergen, Norway

Centre for Climate Dynamics (SKD), Bergen, Norway

Received, 21 October 2011, in final form 7 May 2012

The Ekman boundary layer (EBL) is a non-stratified turbulent layer of fluid in a rotated frame of reference. The EBL comprises two sub-layers, namely, the surface sub-layer, where small scale well-developed turbulence dominates, and the core sub-layer, where large scale self-organized turbulence dominates. This study reports self-organization of large scale turbulence in the EBL as simulated with the large-eddy simulation (LES) model LESNIC. The simulations were conducted in a large domain (144 km in the cross-flow direction, which is an equivalent to about 50 EBL depths) to resolve statistically significant number of the largest self-organized eddies. Analysis revealed that the latitude of the LES domain and, unexpectedly, the direction of the geostrophic wind forcing control the self-organization, turbulence scales, evolution and the quasi steady-state averaged vertical profiles in the EBL. The LES demonstrated destabilization of the EBL turbulence and its mean structure by the horizontal component of the Coriolis force. Visualisations of the EBL disclosed existence of quasi-regular large scale turbulent structures composed of counter-rotating vortices when the geostrophic flow was set from East to West. The corresponding structures are absent in the EBL when the geostrophic flow was set in the opposite (i.e. West to East) direction. These results finally resolve the long-standing controversy between the Leibovich-Lele and the Lilly-Brown instability mechanisms acting in the EBL. The LES demonstrated that the Lilly-Brown mechanism, which involves the vertical component of the Coriolis force, is working in the polar EBL where its impact is nevertheless rather small. The Leibovich-Lele mechanism, which involves the horizontal component of the Coriolis force, acts in low latitudes where it completely alters the turbulent structure of the EBL.

Keywords: atmospheric boundary layer, large-eddy simulations, Ekman boundary layer, turbulence self-organization

1. Introduction

The Ekman boundary layer (EBL) is a non-stratified turbulent boundary layer of fluid in a rotated frame of reference. The frame rotation has several ef-

fects on the EBL turbulence. Firstly, the frame rotation influences a balance of vector forces in the homogeneous steady-state EBL. It is responsible for change of the velocity vector direction with distance from the surface. This resulting velocity profiles is known as the Ekman spiral wind profile (Ekman, 1905). Secondly, it influences the turbulence energy balance of the EBL through redistribution of the energy of fluctuations among components of the velocity vector (Johnston, 1998). In result, variability of the spanwise component of the velocity is significantly enhanced. It leads to additional energy dissipation and a finite steady-state depth of the EBL (Rossby and Montgomery, 1935). Thirdly, the frame rotation skews the eddy vorticity distribution making it asymmetric with respect to the direction of the background frame vorticity. The asymmetry results in the turbulence vorticity vector alignment with the frame vorticity with amplification of the vorticity vectors oriented in the same direction and damping of the vorticity vectors oriented in the opposite directions (Mininni et al., 2009). In the presence of the mean flow vorticity, due to the mean EBL velocity shear, this consequence of the angular momentum conservation law leads to differences in the growth rate of turbulent fluctuations. Through this mechanism, the direction of the geostrophic flow may control the EBL properties. Finally, there are a number of instabilities, which are only indirectly linked to the frame rotation. For instance, the inflection-point instability (Lilly, 1966; Brown, 1970; Etling and Brown, 1993) is caused by the linear Orr-Sommerfeld instability mechanism. This mechanism is acting indirectly, through formation of the Ekman spiral velocity profile, which develops due to the frame rotation.

The interactions between the frame rotation and the EBL structure are nonlinear. In this study, we will investigate them using large-eddy simulation (LES) technique. Previously, fine resolution LES experiments in a large computational domain were inaccessible due to high computational cost of the model runs. This fact limited studies to simplified and linearized models. Constrains on the simplifying assumptions of those models were loose, which resulted in controversial and inconsistent conclusions. We will discuss this controversy throughout the paper.

The simplest model of the frame rotation effects is a Coriolis stability formulation (Bradshaw, 1969; Tritton, 1992; Esau, 2003). The formulation defines a single stability parameter – the Bradshaw-Richardson non-dimensional number, Ri_R, that separates the flow regimes enhanced and suppressed by the frame rotation. One particularly relevant feature of this formulation is the conclusion that the frame rotation additionally destabilizes only the geophysical flows with the component of the horizontal velocity, which is directed from East to West. Such flows will be referred here as EW-flows or easterlies. Contrary, the flows with the component of the horizontal velocity from West to East (WE-flows or westerlies) are unconditionally stable with respect to Ri_R. Although this formulation is instructive, it does not consider the turbulence as such. Hence its applicability to the EBL is to be checked in this study.

A more sophisticated model was proposed by Ekman (1905). It is based on linear ordinary differential equations for the horizontal components of the velocity vector. This model has been studied in many successive works (e.g. Grisogono, 1995; Tan, 2001). The principal assumption of the Ekman model is absence of the horizontal projection of the Coriolis force, which is satisfied in the geophysical flows only at geographical poles with latitude $\varphi = 90^{o}$. Thus, the Ekman model is invariant with respect to the horizontal flow direction. This fact makes the Ekman model inconsistent with the Coriolis stability formulation everywhere except vicinity of the poles. One of the features of the Ekman model is a rotation of the velocity vector direction with height, which is known as the Ekman spiral. The Ekman spiral has been observed both in the atmosphere (e.g. Zhang et al., 2003), the ocean (e.g. Price et al., 1987; Wijffels et al., 1994; Chereshkin, 1995) and in laboratories (e.g. Caldwell et al., 1972; Howroyd and Slawson, 1975) at different latitudes and frame rotation rates. Hence, the Ekman model is applicable not only at the poles as its formulation may suggest. In fact, this model is utilized to parameterize the Coriolis effects in the boundary layer of the large-scale meteorological and ocean models. Therefore, its inconsistency with the EBL turbulence dynamics may have significant implications of the accuracy of weather prediction and climate projections.

As we will recognize in the next Section, the Coriolis force has the largest impact on the largest turbulent eddies in the EBL. The Ekman model accounts for the weighted size of the turbulent eddies implicitly through the eddy viscosity coefficient. This coefficient does not depend on the flow direction and latitude so that it is independent of Ri_R. Hence, traditionally, the eddy viscosity in the EBL is thought as the eddy viscosity of small eddies of the size much less than the EBL thickness. This assumption is inconsistent with a number of studies (e.g. Lilly, 1966; Brown, 1970; Etling and Brown, 1993). The linear stability analysis has shown that the Ekman spiral is directionally unstable with respect to small perturbations. This instability should lead to formation of large-scale vortices (rolls) with the angular velocity vector approximately aligned with the velocity vector of the mean flow. However, this analysis was based on the Ekman model, and therefore, the obtained roll solutions were also independent of Ri_R.

More general linear model, which accounts for both vertical and horizontal components of the Coriolis force, was studied by Leibovich and Lele (1985) and Haeusser and Leibovich (2003). Hereafter it is referred as the Leibovich-Lele model. This model has the solution for the mean flow similar to the solution of the Ekman model. But the stability analysis of this solution is different from the analysis given in Brown (1970). The Leibovich-Lele model also predicts development of large-scale roll vortices in the EBL with the angular velocity vector approximately aligned with the velocity vector of the mean flow. But contrary to Brown's solution, the Leibovich-Lele model predicts dependence of the growth rate of perturbations (turbulence) on Ri_R, i.e on the direction of the mean flow in the EBL. The maximum growth rate is reached in the EW flow. Although in both

models the instability mechanisms in the EBL are linked to the flow direction, the dominant instability mechanism in the Leibovich-Lele model is essentially controlled by the mutual arrangement of the horizontal component of the Coriolis force and the mean flow direction whereas the instability mechanism in the Ekman model is controlled by the rotation of the mean velocity vector with height. Implications of these differences in the instability mechanisms constitute the central part of the discussion in this study.

Although the mentioned EBL models are rather old, their applicability to the geophysical EBL with the complete range of non-linear interactions between the turbulence and the mean flow remains uncertain. Indeed, the models give significantly different predictions only when the Coriolis force effect on the largest eddies (rolls) is considered. The very existence of the rolls in the EBL, leave alone their fine characteristics, is still debatable. The problem is that it is difficult to observe nearly neutral stability flow in the atmosphere and the ocean as well as it is difficult to run laboratory experiments or numerical simulations in a sufficiently large domain to accommodate several rolls. The laboratory experiments are typically conducted in an apparatus too small to allow unaffected self-organization of turbulence (Caldwell et al., 1972). The same statement could be done about direct numerical simulations (Coleman et al., 1990; Spalart et al., 2008). The observations in the atmosphere and the ocean suffer from uncertainties in identification of control conditions. It is recognized that even a slight change in the flow static stability may strongly amplify or suppress the large scale turbulence (Haack and Shirer, 1992; Zilitinkevich and Esau, 2005).

The overall importance of the rolls in the EBL can be estimated only indirectly. Larsen et al. (1985) estimated the energy of the large scale part of the turbulence in a shear driven boundary layer as large as 40% of the total turbulent kinetic energy. Similarly, Barthlott et al. (2007) estimated that the large eddies contributed up to 44% in the total momentum flux and 48% of the heat flux. The impact of large-scale eddies was recognizable during 36% of the total time of long-term atmospheric observations in the surface sub-layer. Kumar et al. (2006) reported a large hysteresis of the turbulent drag in the LES of developing (without large scale structures) and decaying (with the large scale structures) turbulence. This effect was found to be in broad agreement with observations described by Grimsdell and Angevine (2002). Savtchenko (1999) studied the effect of large-eddies on the marine atmospheric surface layer and adjacent underlying wave field combining the Synthetic Aperture Radar (SAR) imagery of ocean surface and the visual range imagery of cloud fields. The data indicated significant degree of coherence between the surface stress and 1 km to 10 km scale turbulent eddies.

The global climatologic assessment of frequency and types of the large scale turbulent structures is even more incomplete and uncertain. The widely cited works by Atkinson and Zhang (1996) and Gerkema et al. (2009) provide very little quantitative information. Recently, Brockmann (http://www.brockmann-consult.de/CloudStructures/index.htm; private communication) made available

global statistics of the boundary layer cloudiness and types of its spatial organization as it was derived from classification of satellite images. Although this classification is ambiguous, it clearly shows that the cloud rolls and streets are ubiquitous in the tropical latitudes. In the ocean upper layer, the large scale turbulent structures were first reported by Soloviev (1990) who observed temperature ramps at 2 m depth in equatorial waters. It seems to be that the large-scale turbulence is more pronounced and more easily found in the low latitudes, which would be inconsistent with the Lilly and Brown analysis but, just opposite, consistent with the Leibovich-Lele model.

In these circumstances, LES model is perhaps the most adequate tool to study the EBL large scale structure. Beginning with pioneering work of Mason and Sykes (1980), the LES and direct numerical simulations (e.g. Beare et al., 2006; Spalart et al., 2008) have been utilized to study this problem. Mason and Sykes (1980) simulated the EBL driven by the WE-flow at mid-latitudes. Although their LES were run in very small domain and were severely under-resolved, they made conclusions in favor to the Lilly and Brown analysis of the Ekman model. Zikanov et al. (2003) conducted the LES of the upper ocean EBL in the equatorial area. He varied the driving flow direction and was able to corroborate the Leibovich-Lele model predictions. Zikanov et al. runs had also rather small domain. It is unclear to what degree the large scale eddies were resolved in those simulations. Huang et al. (2009) studied the effect of a sub-grid scale parameterization on the simulated large scale turbulence. They compared vortices obtained through a truncated principal orthogonal decomposition (POD) analysis of the LES runs in 3142 m by 3142 m by 120 m domain. Esau (2003) used POD to study effects of the frame rotation on the large scale turbulence in his LES.

A new set of fine resolution LES runs in a very large computational domain was produced for this study. Thus, we aim to resolve a statistically significant number of the large scale turbulent eddies in the EBL. These runs span a range of control parameter variability (driving flow directions and latitudes), which will help to assess dependences between the control parameters and the characteristics of the large scale turbulence. This assessment will finally resolve the controversy between the different proposed models of the EBL. Moreover, we will determine the large scale characteristics of the EBL more accurately than it has been possible to date. The next Section 2 sets up mathematical frameworks for the LES result analysis. Here, we will specify the critical parameters of the proposed model and highlight methodology of their falsification with the LES. Section 3 describes the LES code and runs. Section 4 presents the analysis of the simulated EBL. Section 5 outlines conclusions.

2. Mathematical frameworks

A local Cartesian coordinate system (x,y,z) used in the present study is given in Fig. 1. The orts of this system are (i,j,k). The Coriolis force due to the frame rotation is defined as

$$\vec{F}_C = 2\vec{u}\times\vec{\Omega} = 2\begin{bmatrix} i & j & k \\ u & v & w \\ \Omega_x & \Omega_y & \Omega_z \end{bmatrix} = 2\begin{bmatrix} v\Omega_z - w\Omega_y \\ w\Omega_x - u\Omega_z \\ u\Omega_y - v\Omega_y \end{bmatrix} = \begin{bmatrix} f_V v - f_H w \\ -f_V u \\ f_H u \end{bmatrix}. \quad (1)$$

Here, modules of the Coriolis force projections on the vertical, z, and horizontal, y, axis are $f_V = 2\left|\vec{\Omega}\right|\sin\varphi$ and $f_H = 2\left|\vec{\Omega}\right|\cos\varphi$ where φ is the Earth's latitude, $\vec{\Omega} = (\Omega_x, \Omega_y, \Omega_z)$ is the Earth angular velocity vector with $\Omega_x \equiv 0$, and $\vec{u} = (u,v,w)$ is the velocity vector and its projections on the coordinate axes. The velocity vector is equal to the geostrophic velocity vector above the EBL, i.e. $\vec{u} \to \vec{U}_g = (U_g, V_g, 0)$ at $z > h$ where h is the EBL thickness.

Significance of the Coriolis force for fluid motions is determined by the non-dimensional Rossby number $Ro = \left|\vec{u}\right| / L\left|\vec{\Omega}\right|\cos\beta$ where β is the angle between the flow velocity, which is not necessarily geostrophic, and the frame rotation angular velocity (see Fig. 1) and L is the length scale of the motions. The Coriolis force has significant effect when $Ro << 1$ or L is large. In the case of the EBL, the largest length scale is $L = h$ and the smallest Ro will be equal to $Ro = \left|\vec{u}\right| / h\left|\vec{\Omega}\right|$ where $\beta = 0$, i.e. the local velocity of the eddies of the size of the EBL will be aligned with the local direction of the Coriolis force. It immediately implies that the largest effect at the poles the Coriolis force will have on eddies rotating in the horizontal plain whereas the eddies with the rotation in the vertical plain, which are associated with the rolls, should not be affected by the frame rotation. This conclusion is however not applicable to the results of Brown

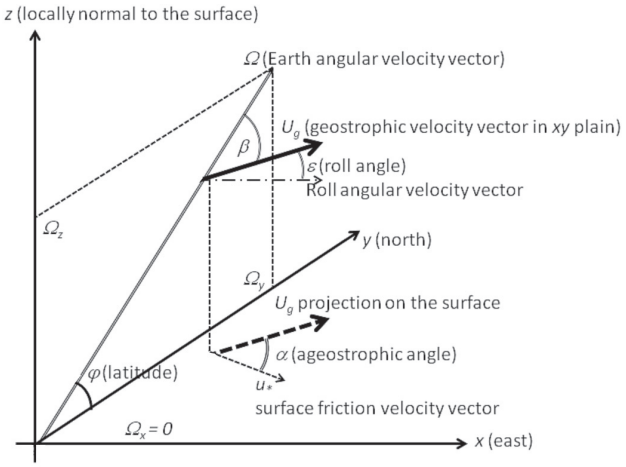

Figure 1. The coordinate system with definitions of the main vectors and angles used in the present study.

analysis as the Coriolis force acts in it indirectly, through the inflection-point instability. More general conclusion from the Rossby number consideration is that the motions must be sufficiently slow. The mixing time scale, $t_{mix} = h/|\vec{u}|$, should be larger than or at least comparable to the Coriolis time scale, $t_f = 1/|\vec{\Omega}| \sim 10^4$ s. In the case of the EBL, $h_{EBL} \propto u_* t_f$ (Zilitinkevich et al., 2007) and therefore $t_{mix} \propto h/u_* = u_* t_f / u_* = t_f$ or $t_{mix}/t_f \sim 1$. In the case of convective boundary layer, the mixing time scale is increasing as $t_{mix} = t^{1/2}$ (e.g. Tennekes, 1973). It may explain the fact of frequent observations of convective rolls (and cloud streets) under strong wind conditions. However, the convective rolls are not necessarily involve the Coriolis forcing (e.g. Haack and Shirer, 1992) and can be observed in laboratory convection without any frame rotation. Moreover, the convective layer depth is often limited by the stability inversion. In such conditions, the convective time scale remains rather small (e.g. Mironov et al., 2000). In the stably stratified boundary layer, the asymptotic mixing time scale is $t_{mix} \propto h/u_* = u_*^2/u_* B_s^{1/2} = u_*/B_s^{1/2}$ where B_s is the module of surface buoyancy flux (Zilitinkevich et al., 2007). As B_s is changing faster than u_*, the mixing time scale t_{mix} decreases, which should make the stably stratified boundary layers paradoxically less sensitive to the Coriolis force effects.

The structure of the EBL is described by the following equation

$$\frac{D\vec{u}}{Dt} + \nabla p' = \vec{F}_C - f_V \vec{U}_g + \vec{F}_T \text{, and } div(\vec{u}) = 0 , \tag{2}$$

where $\vec{U}_g$ is the geostrophic velocity, $\vec{F}_T$ is the friction force. In this study, we will consider only the steady-state EBL, i.e.

$$\vec{F}_C - f_V \vec{U}_g = \vec{F}_T . \tag{3}$$

The Coriolis force does not change the energy balance when integrated over the entire volume of the frictionless flow. But it does redistribute the energy between the velocity components and the different parts within the volume. Mininni et al. (2009) demonstrated this redistribution process in their direct numerical simulations of the homogeneous decaying turbulence in the rotating frame of reference. Their simulations visualize the additive property of the flow vorticity, which receives the direct energy input from the frame rotation when the directions of the frame angular velocity and the local flow velocities are aligned.

The problem formulation can be further simplified when the horizontal homogeneity of the EBL is assumed. In this case, the horizontally averaged vertical component of the flow velocity is $< w > = 0$ due to $div(\vec{u}) = 0$ constraints. Additionally assuming a flux-gradient relationship in the form

$$\vec{F}_T = -\nu_t(z) \frac{d < \vec{u} >}{dz} , \tag{4}$$

where the effective eddy viscosity $\nu_t(z)$ can be defined through the bulk energy dissipation in the EBL, we arrive to the classical Ekman problem (Ekman, 1905; Miles, 1994; Tan, 2001)

$$f_V(<\vec{v}> - <\vec{V}_g>) = -\frac{d}{dz}\nu_t(z)\frac{d<\vec{u}>}{dz}, \tag{5a}$$

$$f_V(<\vec{u}> - <\vec{U}_g>) = \frac{d}{dz}\nu_t\frac{d<\vec{v}>}{dz}. \tag{5b}$$

The solution of Eq. (5) is given in Grisogono (1995) and Tan (2001) in the form

$$<u> = u_g(1 - A(z)e^{-F(z)}\cos F(z)) - V_g A(z)e^{-F(z)}\sin F(z), \tag{6a}$$

$$<v> = v_g(1 - A(z)e^{-F(z)}\cos F(z)) + U_g A(z)e^{-F(z)}\sin F(z), \tag{6b}$$

where

$$F(z) = (f/2)^{1/2}\int_0^z \nu_t^{-1/2}(\varsigma)d\varsigma, \tag{6c}$$

$$A(z) = \left(\nu_t(0)/\nu_t(z)\right)^{1/4}. \tag{6d}$$

This solution is different from Ekman (1905) due to the variability of ν_t with altitude. One can obtain the classical Ekman solution taking $A(z) = 1$ and $F(z) = z/\delta$, where $\delta = \left(2 <\nu_t> / f_V\right)^{1/2}$ is the EBL thickness scale.

The solution (6) involves only a very small set of control parameters. They are: latitude, φ; the geostrophic wind speed, $U = \left|\vec{U}_g\right|$; and the effective eddy viscosity $\nu_t(z)$. The shape of profiles determines specific values of the EBL parameters, e.g. $\nu_t(z) \to 0$ with height reduces the surface ageostrophic angle $\alpha = \tan^{-1}(<v(0)> / <u(0)>)$ from 45°, as in Ekman (1905) for the constant $<\nu_t(z)>$, to less than 15°, as it is obtain in LES and observations. But variations of the $\nu_t(z)$ shape do not add new qualitative features to the model.

The analytical solution (6) is linearly unstable with respect to infinitesimal perturbations in the turbulent flow (e.g. Lilly, 1966; Brown, 1970; Etling and Brown, 1993). This instability is referred to as the inflection-point instability since it appears due to the inflection of the mean velocity profile of the Ekman spiral in a certain direction. Observe that this stability analysis is linked to the Coriolis force only indirectly, through the role of f_V in the Ekman spiral formation. Significance of the instabilities of the solution (6) with respect to the complete non-linear problem in Eq. (2) cannot be established without observations of the natural EBL or the numerical solution of Eq. (2) by the LES model.

It is however possible to obtain a solution of the homogeneous linearized problem in Eq. (3), which accounts for the full Coriolis force with f_V and f_H

components. This analysis is given in Leibovich and Lele (1985) and Haeusser and Leibovich (2003). Here, we will not repeat their lengthy mathematical derivations as the purpose of this study is to compare the LES results with the conclusions obtained via the analytical stability analysis of the linearized models. Therefore, instead of the detailed analysis of the Leibovich-Lele model, we move to simplified but equally illuminative analysis introduced by Bradshaw (1969) and Tritton (1992).

Bradshaw (1969) considered effects of the total vorticity conservation in a rotating fluid volume. He noted that flow perturbations should either reduce of increase the flow vorticity depending on alignment between the vorticity and the frame angular velocity. This effect of the frame rotation on the turbulent energy cascade is known as the Coriolis stratification. By analogy with the density stratification, it could be measured with a non-dimensional Bradshaw-Richardson number (Tritton, 1992; Salhi and Cambon, 1997; Esau, 2003), which is written as

$$Ri_R = S(S+1), \text{ where } S = \frac{-2\omega_{eff}}{\omega_{shear}}. \tag{7}$$

Here $\omega_{shear} = \left|\vec{\nabla}\times\vec{u}\right|$ is the module of the shear induced vorticity. If $\vec{n}$ denotes the vorticity direction, than the scalar product $\omega_{eff} = \left(\vec{F}_C \bullet \vec{n}_\perp\right)$ is a projection of the Coriolis force on the direction normal to the local vorticity vector. One may say that the flow is locally stabilized by the Coriolis force when $Ri_R > 0$. It means that a fluid particle displaced along $\vec{n}$ in either direction feels a restoring force, which tends to return the particle to its original location. In the stabilized flow, turbulent perturbations are damped and the Reynolds stress is reduced. Correspondigly, the flow is locally destabilized when $Ri_R < 0$, which means that the displaced particle tends to increase its initial displacement.

Eq. (7) is quadratic with respect to S. The neutral conditions, $Ri_R = 0$, are achieved at $S = 0$ ($\omega_{eff} = 0$; the local Coriolis force is orthogonal to the flow vorticity) and at $S = -1$ ($\omega_{shear} = 2\omega_{eff}$). The maximum instability is attained at

$$\frac{\partial Ri_R}{\partial S} = 2S + 1 = 0, \text{ which gives } Ri_R = -\frac{1}{4},\ S = -\frac{1}{2} \text{ and } \omega_{shear} = 4\omega_{eff}. \tag{8}$$

Fig. 2 shows that the sheared parallel flow becomes unstable only within a narrow range of S. In the case of the horizontally homogeneous EBL, $\vec{n}$ is aligned the with $\vec{k}$, so that the flow vorticity becomes

$$\vec{\omega}_{shear} = \vec{\nabla}\times\vec{u} = \begin{bmatrix} i & j & k \\ \partial/\partial x & \partial/\partial y & \partial/\partial z \\ u & v & w \end{bmatrix} = \begin{bmatrix} i & j & k \\ 0 & 0 & \partial/\partial z \\ u & v & 0 \end{bmatrix} = \begin{bmatrix} -\partial v/\partial z \\ \partial u/\partial z \\ 0 \end{bmatrix}, \tag{9}$$

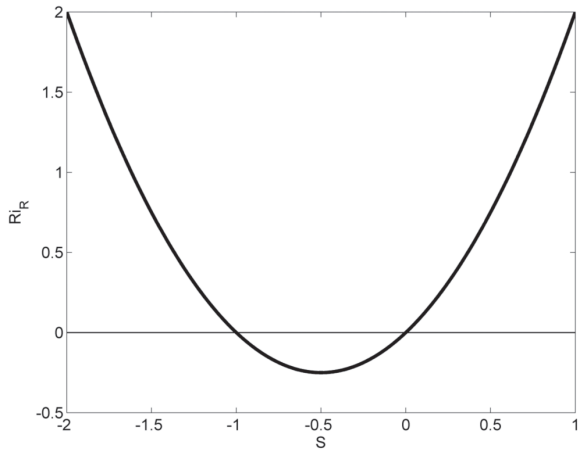

Figure 2. The flow Bradshaw-Richardson stability number, Ri_R, as function of the relative vorticity parameter S after Eq. (7).

For a zonal flow in the Northern Hemisphere, i.e. $\vec{U}_g = (\pm U, 0)$, one can obtain

$$\omega_{shear} = \partial U / \partial z > 0, \text{ for } U > 0 \text{ (WE-flows or westerlies) and}$$

$$\omega_{shear} < 0, \text{ for } U < 0 \text{ (EW-flows or easterlies).} \tag{10}$$

The projection of the Coriolis force on such a zonal flow is

$$\omega_{eff} = -\left(\vec{F}_C \bullet [i, j, 0]\right) = -\left(\Omega_x i + \Omega_y j\right) = -\Omega_y, \tag{11}$$

where the minus sign accounts for the Earth's counter-clockwise rotation. We can obtain the dependence between $\mathrm{Ri_R}$ and the velocity shear, U / δ_s, across the surface layer of thickness δ_s. In this case, we have

$$S = \frac{-2\delta_s(-\Omega\cos\varphi)}{\pm U}. \tag{12}$$

Fig. 3 presents this dependence for U = 10 m s^{-1} and δ_s = 100 m ($\delta_s \sim 0.05$ δ). The figure illustrates that perturbations in the westerlies are always damped by f_H, and therefore, its exclusion out of consideration may lead to misleading conclusions about the EBL structure and stability. Fig. 4 generalize these results presenting the stability analysis for EW-flows and WE-flows. The neutral stability in terms of Ri_R is marked with the red line. It is clearly seen that only the EW-flows (easterly winds) and only sufficiently strong wind shear, which also depends on latitude, cause the Coriolis instability in the EBL when large scale eddies could be forced directly by the frame rotation. At the same time, any flow,

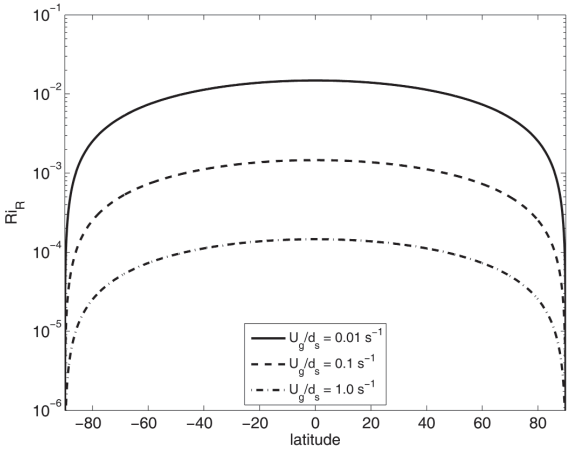

Figure 3. The flow Bradshaw-Richardson stability number, Ri_R, as function of latitude after Eq. (12) for the WE-flow (westerlies): the bold line represents the shear $U/\delta_s = 0.01$ s^{-1}; the dashed line is $U/\delta_s = 0.1$ s^{-1}; the dash-dotted line is $U/\delta_s = 1$ s^{-1}. The neutral stability is reached at the poles and the maximum stability – at the equator.

independent of its direction and velocity shear, has the neutral Coriolis stability at the poles.

The presented brief framework analysis gives us a possibility to confront, and therefore to falsify, the existing linearized models. However, validity of the model's assumptions cannot be judged in frameworks of the given models. The judgment requires analysis of the behavior of the complete non-linear EBL. This behavior will be obtained through a set of LES runs. Tab. 1 summarizes key differences in predictions of the considered models. It confronts the conclusions

Table 1. Predictions of the control parameters corresponding to the maximum turbulent kinetic energy and the most energetic length scale of eddies in the flow.

f_V-mechanisms	f_H-mechanisms	Zero-hypothesis
EBL at the poles, $\varphi = 90°$	EBL at the equator, $\varphi = 0°$	Indifferent to the latitude
Indifferent to the geostrophic wind direction	EBL driven by the East to West (easterly) winds	Indifferent to the flow direction
Spiral wind profile in the EBL is essentially perturbed	Insignificant perturbations of the spiral wind profile in the EBL	Insignificant perturbations of the spiral wind profile in the EBL
The most energetic eddies comprise the entire EBL; their horizontal scaling is height-independent	The most energetic eddies comprise the entire EBL; their horizontal scaling is height-independent	The most energetic eddies comprise only the surface sublayer; their horizontal scaling increases with height

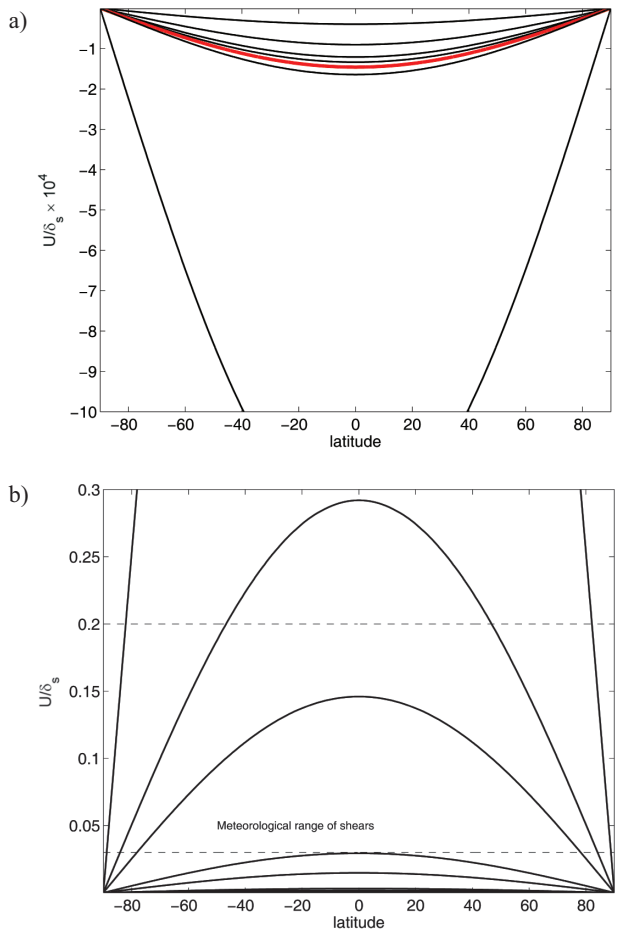

Figure 4. The flow Bradshaw-Richardson stability number, Ri_R, as function of latitude and velocity shear across the surface layer, U / δ_s; (a) the EW-flow with unstable Ri_R contours –0.25 and –0.1 (dashed lines), the neutral Ri_R contour 0 (bold red line), and stable Ri_R contours 0.1, 0.25, 1.0, 10 (solid lines); (b) the WE-flow with stable contours $0 \cdot 10^{-4}$, $5.0 \cdot 10^{-4}$, 10^{-3}, $5.0 \cdot 10^{-3}$, 10^{-2}, $5.0 \cdot 10^{-2}$, 10^{-1}, and 0.25 (solid lines).

of the Brown analysis (only f_V component of the Coriolis force is taken into account), the Leibovich-Lele analysis (both f_V and f_H components are taken into account), and, in addition, a zero-hypothesis. The zero-hypothesis states that the Coriolis force has the effect only on the mean flow structure in the EBL but the EBL turbulent structure is determined by the velocity shear only. The zero-hypothesis comes from observations and simulations of the boundary layer flows in non-rotated frames of reference. The large scale turbulence in such sheared flows is also organized in a sort of rolls with the vorticity vector nearly parallel

to the mean flow velocity vector. This apparent similarity between the structures in the EBL and in the non-rotated boundary layers has been used to explain the properties of the former one by several authors (e.g. Lin et al., 1996; 1997; Drobinski and Foster, 2003; Foster et al., 2006).

3. The large-eddy simulation experiments

The LES code LESNIC (abbreviation for the Large Eddy Simulation Nansen centre Improved Code) was used to obtain the turbulence structure and interactions in the idealized EBL over the homogeneous flat surface. LESNIC (Esau, 2003; Esau, 2004; Esau and Zilitinkevich, 2006) solves the Navier-Stokes equations for incompressible Boussinesq fluid (e.g. Zeytounian, 2003). It is convenient to use Einstein's tensor notation to describe the governing equations of the LES model. Let us define $u_i = (u,v,w)$. We also introduce dynamic pressure p as deviation from the hydrostatic pressure. The incompressibility condition reduces the continuity equation to the non-divergence equation, which is solved by the accurate direct Fourier transformation method. This pressure solver requires the periodic lateral boundary conditions in the model domain. Thus, the largest resolved motions in the domain are restricted by the domain half-size whereas the smallest resolved motions are restricted by the double grid cell size.

The LESNIC equations are

$$\partial u_i / \partial t = -\partial / \partial x_j (u_i u_j + \tau_{ij} + p\delta_{ij}) - 2\Omega_j \varepsilon_{ijk} u_k \,, \tag{13a}$$

$$\partial u_i / \partial x_i = 0 \,, \tag{13b}$$

where δ_{ij}, ε_{ijk} are the Kroneker delta and the unit alternating tensors. The turbulent stress tensor τ_{ij} is responsible for the energy dissipation in the model. To construct τ_{ij}, LESNIC utilizes an analytical solution of a simplified variation optimization problem for the spectral energy transport in the inertial sub-range of scales (for the detailed description see Esau, 2004). The essence of the problem is to find such values of τ_{ij}, which will balance the amount of energy cascading through the mesh scale, Δ, with the amount of energy cascading through some larger resolved scale, $\Delta^L > \Delta$. The latter value can be explicitly computed as L_{ij}^L (see below) up to accuracy of the numerical scheme. In a nearly laminar flow, L_{ij}^L is sufficient for the spectral turbulence closure as there is no sub-grid scale turbulence to interact with the resolved scale turbulence. The problem is more complicated in the well developed EBL. Here, a large fraction of energy is cascading indirectly through interactions between motions with significantly different scales, including those with unresolved scales. In this case, the magnitude of L_{ij}^L is not sufficient to describe the spectral energy transport. The magnitude of L_{ij}^L saturates at about 50% of the total turbulent stress magnitude (Sullivan et al., 2003). Therefore, L_{ij}^L must be complemented with an additional parameteriza-

tion of the purely dissipative Smagorinsky stress tensor (Vreman et al., 1997). LESNIC employs a reduced dynamic-mixed model, which is expressed as

$$\tau_{ij} = L_{ij}^{L} - 2l_s^2 \left|S_{ij}\right| S_{ij}, \tag{14a}$$

$$l_s^2 = \frac{1}{2}\frac{\left(L_{ij}^{L} - H_{ij}^{L}\right) \bullet M_{ij}^{L}}{M_{ij}^{L} \bullet M_{ij}^{L}}, \tag{14b}$$

$$L_{ij}^{L} = \left(u_i u_j\right)^{L} - \left(u_i\right)^{L}\left(u_j\right)^{L}, \tag{14c}$$

$$H_{ij}^{L} = \left(\left(\left(u_i\right)^{L}\left(u_j\right)^{L}\right)^{l}\right)^{L} - \left(\left(\left(u_i\right)^{L}\right)^{l}\right)^{L}\left(\left(\left(u_j\right)^{L}\right)^{l}\right)^{L} - \left[\left(\left(u_i\right)^{l}\right)^{L}\left(\left(u_j\right)^{l}\right)^{L} - \left(\left(u_i\right)^{l}\left(u_j\right)^{l}\right)^{L}\right], \tag{14d}$$

$$M_{ij}^{L} = \left(\left|S_{ij}\right| S_{ij}\right)^{L} - \alpha\left|\left(S_{ij}\right)^{L}\right|\left(S_{ij}\right)^{L}, \tag{14e}$$

$$S_{ij} = \frac{1}{2}\left(\partial u_i / \partial x_j + \partial u_j / \partial x_i\right). \tag{14f}$$

Here $A_i \bullet A_j$ is the scalar product, $\left|A_i\right| = \left(A_i \bullet A_i\right)^{1/2}$, the superscripts l and L denote filtering with the mesh length scale and the twice mesh length scale filters. The filters' squared aspect ratio is $\alpha = 2.92$ for the Gaussian and the top-hat filters, which are undistinguishable when discretized with central-difference schemes of the 2nd order of accuracy. The reader should observe that the formulation in Eq. (14b) for the mixing length scale is given in quadratic form. It implies imagery values for the mixing length in certain flow conditions. The physically meaning of these imagery values is that the turbulence energy is cascading back from the small to large scales of motion. The tensors in the closure (14) are: τ_{ij} is the parameterized turbulent stress; L_{ij}^{L} is the part of τ_{ij}, which is due to interactions between the resolved scale motions only; H_{ij}^{L} or the cross term is the part of τ_{ij}, which describes the interactions between the resolved scales with the effect on the unresolved scales of motions; M_{ij}^{L} or the sub-grid term is the part of τ_{ij}, which the interactions with the direct effect on the unresolved scales of motions; and S_{ij} is the resolved velocity shear tensor. It is worth to observe that L_{ij}^{L} and H_{ij}^{L} are independent of the choice of the turbulence closure but depend on the choice of the model filter and the optimization method. The exact form of M_{ij}^{L} depends on the turbulence closure.

LESNIC uses the 2nd order fully conservative finite-difference skew-symmetric scheme, the uniform staggered C-type mesh, and the explicit Runge-Kutta 4th order time scheme. Their detailed description can be found in Esau (2004).

In this study, the LESNIC experiments were run in a quasi two-dimensional domain. This choice is defined by the limited computational resources and the needs to resolve a statistically significant number of the large scale turbulent

eddies in the computational domain. The domain geometric size was 0.3 km in the streamwise direction, 144 km in the cross-flow direction, and 3 km in the vertical direction. The model mesh had 8×4096×128 grid nodes in the corresponding directions. Thus, the small scale turbulence was well resolved in all directions. The large scale turbulence was restricted in the streamwise direction and, in some cases, in the vertical direction. Such a model domain was chosen to focus on the investigation of the streamwise oriented rolls as the dominant large scale structure in the EBL, which is suggested by the considered analytical models. Possible instabilities (e.g. the elliptical instability), which are significantly inhomogeneous in the flow streamwise direction, have not been studied.

The surface boundary conditions in LESNIC are

$$\tau_{i3}(x,y,z=0) = u_*^2(x,y)\cdot u_i(x,y,z_1)/\left|u_i(x,y,z_1)\right|,\ i=1,2, \tag{15a}$$

$$u_*(x,y) = \kappa\left|u_i(x,y,z_1)\right|/\ln(z_1/z_0), \tag{15b}$$

$$\tau_{i3}(x,y,z=L_z) = 0, \tag{15c}$$

$$\partial u_i/\partial z\Big|_{z=L_z} = 0. \tag{15d}$$

Here, $z_0 = 0.1$ m is surface roughness, $\kappa = 0.4$ is the von Karman constant, L_z is the height of the domain. The runs were integrated for 12 hours. The data were sampled every 600 s, processed and averaged over successive one hour intervals. The geostrophic wind speed was set to $U = 5$ m s^{-1}. The control parameters modified in this set of runs were latitude and the geostrophic wind direction (see Tab. 2).

4. The large-scale structure of the EBL

4.1. The vertical structure of the EBL

We begin the presentation of results with analysis of the mean flow structure during the last hour of simulations. Fig. 5 shows the velocity hodographs in the simulated EBL. As compared to three-dimensional LESNIC runs from DATA-

Table 2. Varied parameters, abbreviations of the LESNIC runs and corresponding symbols.

	Westerlies (flow directed from West to East)	Easterlies (flow directed from East to West)
The North Pole domain, φ = 90° N	A0U5L90 (open squares)	A180U5L90 (open circles)
The near Equatorial domain, φ = 5° N	A0U5L5 (closed squares)	A180U5L5 (closed circles)

BASE64 (Esau and Zilitinkevich, 2006), the present quasi two-dimensional LESNIC runs show slightly smaller geostrophic angles. In high latitudes (open circles and squares), the normalized cross-flow velocity component $v/\left|\vec{U}_g\right|$ reaches only about 0.2, which is in reasonable agreement with the fully three-dimensional runs. The wind hodographs of the westerly and easterly flows are almost the same. This is not the case at low latitudes where one can observe a pronounced difference between the wind hodographs in the westerly and the easterly flows (closed circles squares). Contrary to the Etling and Brown (1993) opinion, the well developed Ekman spiral was found in the mean wind profiles in all runs.

The mean vertical profiles of the normalized turbulent kinetic energy (TKE) and the effective dimensional eddy viscosity, $\nu_t^{eff} = \left|\tau_{ij}\right| / \left|d\bar{u}/dz\right|$, are shown in Fig. 6. In high latitudes, the profiles (open circles and squares) are almost identical. It suggests that the EBL structure is independent of the flow direction. In low latitudes, the profiles (closed circles and squares) are very different. The TKE is considerably smaller in the WE-flow. The drastic increase of the TKE in the EW-flow suggests that such flows excite some sort of instability, which pumps energy into the turbulent fluctuations. The effective viscosity behaves differently. It is considerably reduced in the EBL driven with the EW-flow. Thus, the additional TKE is concentrated on the scales, which do not influence the turbulent dissipation. It suggests that the EBL with easterlies should possess large scale turbulent structures and that those structures should be spectrally separated from the small scale dissipative turbulence. This interpretation is consistent with the formulation of the dynamic-mixed sub-grid scale closure in LE-

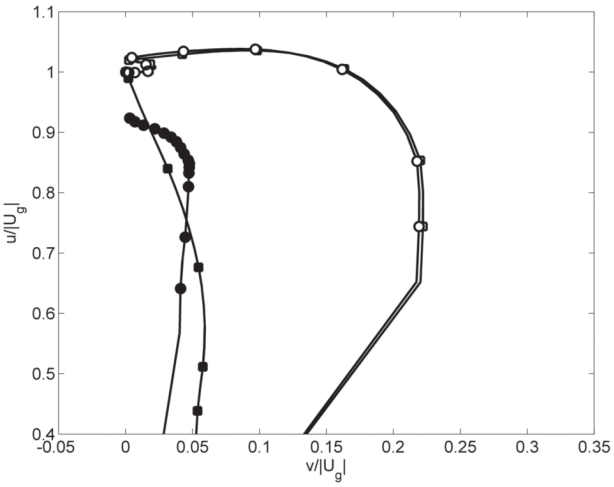

Figure 5. The EBL wind speed hodograph in the present LESNIC simulations. The LES runs are gives as in Tab. 2: A0U5L90 (open circles); A180U5L90 (open circles); A0U5L5 (closed circles); A180U5L5 (closed circles).

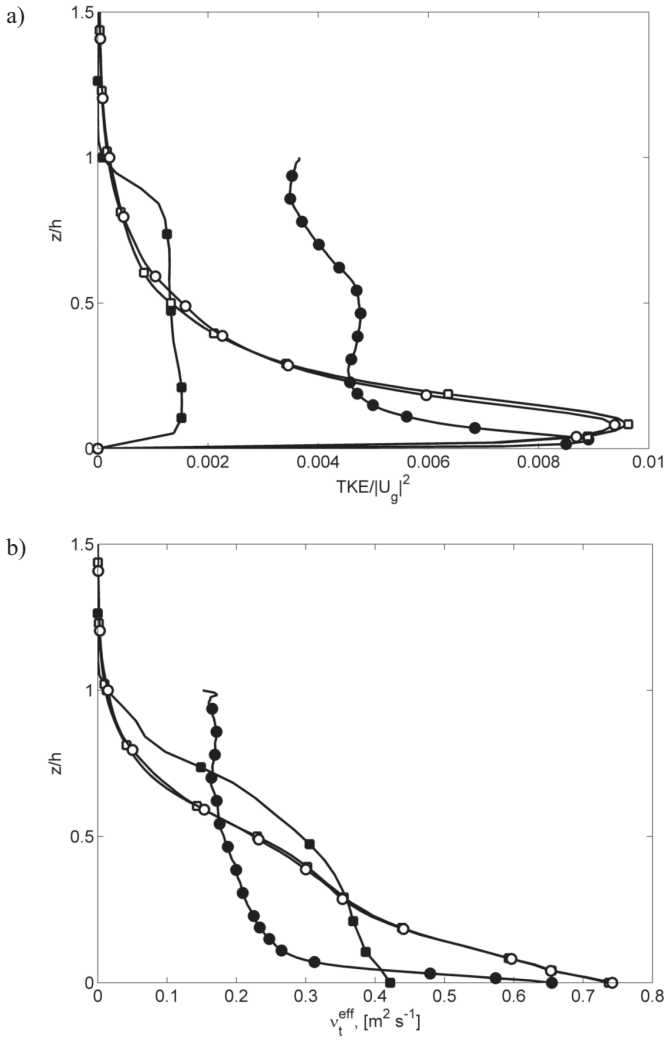

Figure 6. The vertical structure of the simulated EBL: (a) normalized profile of the turbulent kinetic energy (TKE); (b) the dimensional profile of the effective eddy viscosity. The EBL thickness h is defined as the height where the turbulent Reynolds stress drops to 1% of its surface value. The EBL thickness h should not be confused with the EBL thickness scale δ (see in text for details). The LES runs are marked as described in Fig. 5 and Tab. 2.

SNIC. The LESNIC turbulent stress (the nominator in the eddy viscosity formulae) is the function of the TKE at the smallest resolved scales. Thus, the increase of the TKE and the simultaneous decrease of the eddy-viscosity in the run A180U5L5 should indicate amplification of the turbulent motions, which are much larger than the doubled grid spacing in the model. This observation match-

es the f_H-mechanism (Leibovitch and Lele, 1985) but inconsistent with both the f_H-mechanism and the zero-hypothesis. The reader should observe that the simulation domain was too shallow to accommodate the entire EBL driven by the easterly winds at the low latitudes. Fricke (2011) studied this problem with fully three-dimensional simulations using the PALM code. He found that the primary large scale turbulent eddies occupy roughly 3 km to 4 km layer but weaker counter-rotating secondary eddies were found on the top of them. The secondary eddies occupied the layer up to 7 km height and they were probably still restricted by the domain size. Thus, the thickness of the EBL at low latitudes cannot be defined unambiguously. This observation is in agreement with the Ekman conclusion that the EBL depth is scaled as $(f_V)^{-1/2}$.

4.2. The time evolution of the EBL

A look at the EBL time evolution will disclose whether there are any periods with exponentially growing instabilities or large temporal fluctuations in the TKE. Such oscillations and rapid growth periods have been suggested by some linearized models (e.g. Ponomarev et al., 2007). Our simulations do not reveal such effects. Fig. 7 shows the temporal evolution of the four simulated EBLs. In all runs, the TKE grows steadily over the 12 hour period. We rerun the A180U5L5 experiment for 43 hours of model time. This run does not show any significant fluctuations of the TKE. The TKE saturates after about 15–18 hours of simulations with no oscillations during the following hours. The TKE in the other runs saturates much earlier after 6 to 8 hours of the model time.

The EBL thickness in the high latitudes is limited by the Ekman scale $\delta = (2\nu_t / f)^{1/2}$ where the effective eddy viscosity can be expressed using Rossby and Montgomery (1935) relationship $\nu_t = (C_R u_*)^2 / 2f$. The constant C_R has been discussed in meteorological literature for decades until Zilitinkevich et al. (2007) fitted it with LESNIC runs to be $C_R = 0.65$. This fit was obtained in the EBL driven with the WE-flow. As this study suggests, the Rossby-Montgomery constant is sensitive to the flow direction and latitude as well. In low latitudes, the Ekman scaling is not applicable and there are presently no reasonable estimations of the EBL thickness. Analysis of the present and Fricke (2011) LES does not provide a clear idea whether the EBL thickness is limited in the low latitudes and whether f_H and the geostrophic wind direction can scale it. The f_H-mechanism neither extracts nor pumps energy into the turbulence in high latitudes. Therefore, the development of the TKE in both polar runs is nearly the same. The f_H-mechanism works in the low latitudes. It is clearly seen in Fig. 7 where the TKE is amplified in the easterly flow but damped in the westerly flow. Hence, this amplification/damping of the TKE should be attributed to the f_H-mechanism.

Surprisingly, the pronounced difference in the TKE is reflected in the geostrophic drag coefficient and in the surface stress only partially. Fig. 8 shows the time evolution of the geostrophic drag coefficient, $C_g = \left(u_* / \left|\vec{U}_g\right|\right)^2$. The coefficients

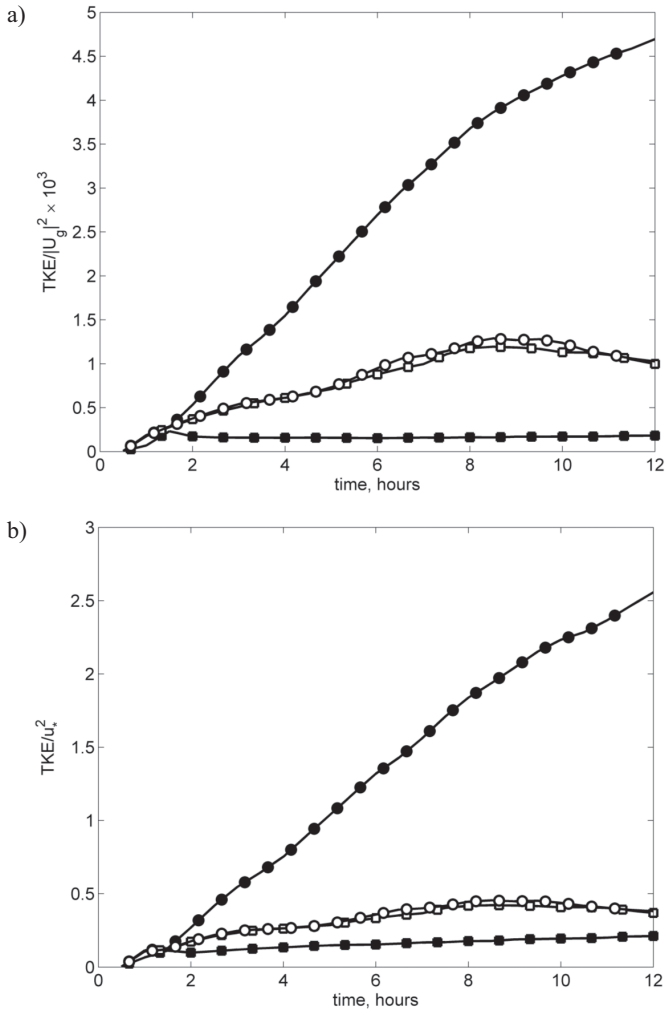

Figure 7. Temporal evolution of the domain averaged turbulent kinetic energy (TKE) normalized by: (a) the module of the geostrophic velocity; (b) the surface friction velocity. The LES runs are marked as described in Fig. 5 and Tab. 2.

differ by factor of 2 among the runs that corresponds to the friction velocity differences by less than 50%. The corresponding TKEs differ by almost one order of magnitude. Moreover, C_g does not follow the pronounced growth of the TKE in the run A180U5L5. This peculiar behaviour of the surface turbulent stress with respect to the TKE refers to the conception of inactive turbulence (Townsend, 1961). According to this conception, large and energetic turbulent eddies are detached from the surface and do not exert significant turbulent stress on it. This

peculiar behaviour is inconsistent with our zero-hypothesis. It is known that the large structures in the sheared layer (streaks) are responsible for a considerable fraction (20% to 40%) of the total surface Reynolds stress (Schoppa and Hussain, 1998). The more detailed discussion of the surface layer turbulence in our runs is out of scope of the present study.

4.3. The large-scale eddy structure of the EBL

The comparative analysis of the mean and integral parameters of the LESNIC runs suggested that the EBL structure among the four runs should be rather different. Moreover, the differences should be found in the large scale turbulence organization. Here, we will visualize the EBL structure and will estimate scales of the most energetic turbulent eddies. Fig. 9 presents an instant cross-flow section (the first 36 km out of the total 144 km of the cross-flow domain size) of $< w >_x$ where $< \cdot >_x$ denotes averaging in the streamwise domain direction. This EBL cross-flow section of the run A180U5L5 reveals the large scale turbulence self-organization in the almost regular vortex pattern. This pattern consists of counter-rotating rolls aligned in the flow streamwise direction. The following features are to be mentioned:

- The roll cross-flow length scale, λ, is about 3 km. It corresponds to the EBL thickness scale, $\lambda = \delta$, so that the aspect ratio between the horizontal and vertical scales of the roll is close to unity.
- The roll length scale λ is independent of altitude. This observation is inconsistent with the zero-hypothesis, which suggests the streak scaling should

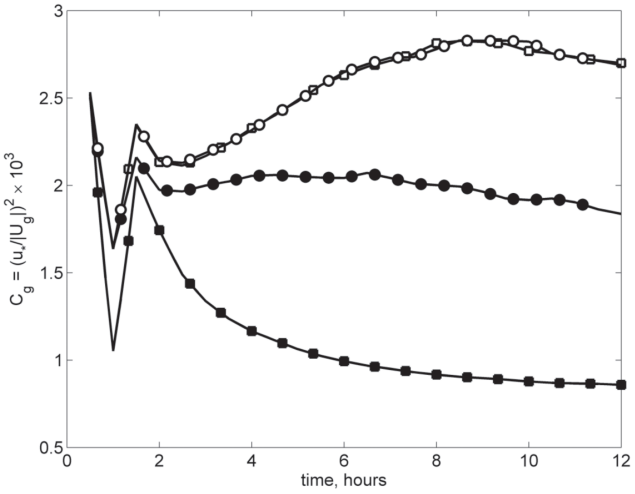

Figure 8. The time evolution of the geostrophic drag coefficient. The LES runs are marked as described in Fig. 5 and Tab. 2.

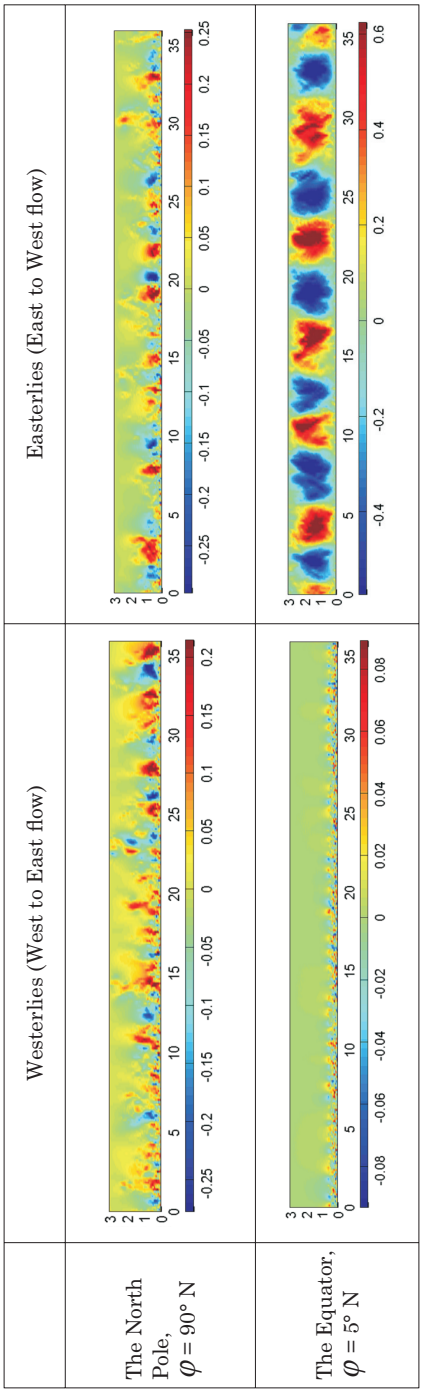

Figure 9. The instant cross-flow sections of the vertical component w [m s^{-1}] (colour shading) of velocity averaged in the streamwise direction. The distances on the y-axis (the horizontal cross-flow axis) and the z-axis (the vertical axis) are given in km. Panels are given for LES runs as listed in Tab. 2. The negative values of w correspond to downward motions.

be linearly proportional to the distance from the surface (Lin et al., 1996; 1997).

- The turbulence in the polar EBLs is organized in less regular and less energetic vortices but it does keep some similarity to the rolls.
- The turbulence in the low latitude EBL driven with WE-flow (the run A0U5L5) does not show recognizable large scale self-organization.
- In the sense of the large scale turbulence self-organization, the run A180U5L5 is rather different from all other runs.

The primary question to the turbulence pattern in the EBL is whether there is a single dominant pattern of turbulence, which could be attributed to a single dominant instability mechanism. Fig. 10 shows the analysis of vertical momentum flux autocorrelations. The analysis itself is described in the Appendix. The correlation length scale in the run A180U5L5 is defined quite certain. The largest anti-correlation is reached at the normalized distance $\lambda / \delta = 1$. The EBL thickness is well identified in this analysis as the height where the anti-correlation length scale drastically increases by an order of magnitude. This height corresponds to $z / h = 0.9$ where h is the EBL thickness independently defined as the height where the turbulent momentum flux drops below 1% of

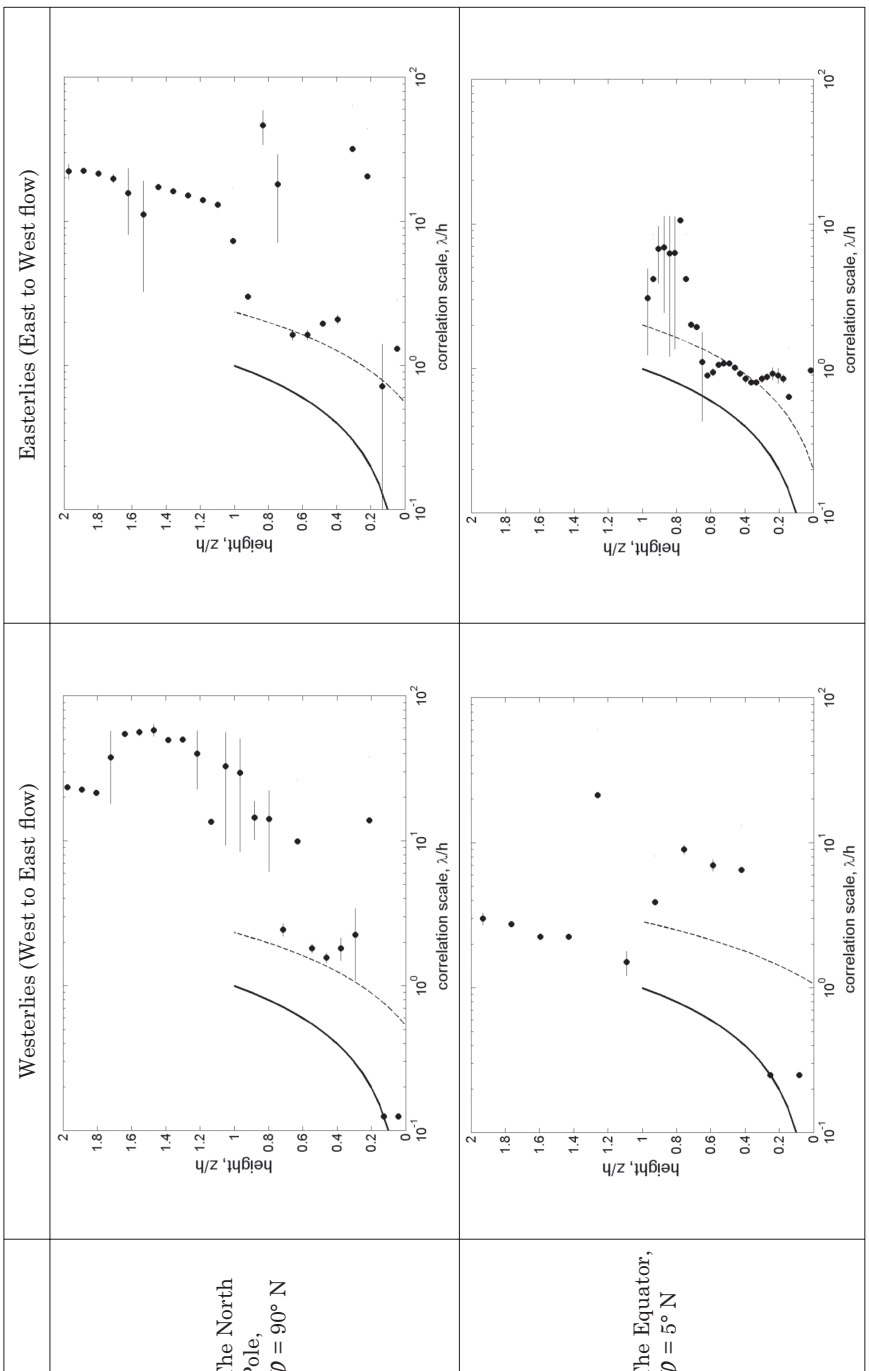

Figure 10. The vertical profiles of the correlation length scale λ. Thze length scale is defined as in the Appendix. Panels are given for LES runs as listed in Tab. 2. The horizontal bars represent one standard deviation of λ, computed for different cross-flow sections. The solid line is the scaling $z = \lambda$; the dashed line is the linear scaling $z/h = a\,\lambda\,/\,h + b$ proposed in Lin et al. (1996) with coefficients $a = 600\,/\,h$ and $b = 1.8$.

its surface value. The run A0U5L5 does not show any certain correlation scale within the EBL as well as it does not show any clear transition of the length scales between the EBL and the flow above it. The correlation length scale analysis for the polar runs is less certain than the corresponding analysis for the run A180U5L5 but the EBL core (between $z/h = 0.2$ and 0.8) with the height-independent scale $\lambda = \delta$ is recognizable. The transition to larger correlation scales above the EBL is easy to observe.

The analysis of the large scale cross-flow turbulence patterns confirmed the development of the energetic regularly organized rolls in the low-latitude EBL driven by the EW-flow (easterlies). It is worth to mention that the easterlies are the dominant winds in the lower atmospheric layers in the low latitudes. Hence, the EBL rolls might have considerable importance for the weather forecast and climate predictions. There is very pronounced contrast between the EW-flow and WE-flow turbulence organization in the low latitude EBL. This contrast strongly supports the attribution the f_H-mechanism as the dominant instability mechanism in the EBL. Thus, the LES experiments corroborate the Leibovich-Lele model. However, the other mechanisms of instability are not excluded. The polar EBLs revealed some degree of self-organization. Since the f_H-mechanism does not work on the poles, the observed semi-regular structure of the large scale turbulent vortices should be attributed to the f_V-mechanism. This structure cannot be attributed to the zero-hypothesis as the vortex scaling does not show significant dependence on the height above the surface. Nevertheless, we cannot exclude the zero-hypothesis either. All runs show reduction of the correlation scales in the surface sub-layer (the lowest 20% of the EBL). The zero-hypothesis (the streamwise vortex growth due to the action of the velocity shear) is probably the dominant mechanism of instability in the surface sub-layer. Here, the velocity shear is large and the turbulent scales are small so that the Coriolis force does not have significant effects.

5. Conclusions

The Ekman boundary layer (EBL) is a non-stratified turbulent boundary layer in a rotating frame of reference. The mathematical description of the steady-state EBL over the homogeneous flat surface is rather simple. This apparent simplicity of the description is however illusive. Firstly, the explicit analytical solution of the EBL equations with a realistic effective eddy viscosity profile is not available. Secondly, the proposed analytical steady-state EBL models were proved to be unstable (both linearly and non-linearly) with respect to the EBL turbulent perturbations. In other words, infinitesimal turbulent perturbations will amplify certain growing modes and there is no mechanism in the linearized EBL models to limit this growth. Moreover, the different linearized EBL models disagree on the dominant instability mechanism in the EBL as well as on its relation to the Coriolis force. Hence, the models also disagree on the

parameters, which control the EBL characteristics and structure. As the atmospheric (ocean) observations and the laboratory experiments were proved to be inconclusive, a set of numerical LES experiments with the LESNIC code was run to resolve the controversy presented by the analytical model analysis.

The LESNIC runs simulated the EBL in a quasi two-dimensional domain, i.e. the large scale turbulence was resolved in the vertical (the size of 3 km) and cross-flow (the size of 144 km) directions of the domain. The size of the streamwise domain direction was only 0.4 km. Thus, it has been implicitly assumed that the EBL structures of interest are homogeneous in the streamwise direction such as the longitudinal rolls, which has been predicted by all considered analytical models. The small scale turbulence was fully resolved down to the grid cell size. Hence, the turbulent energy cascade in the inertial sub-range of scales was not significantly disturbed by the domain configuration. Four LESNIC runs were analyzed (see Tab. 2).

In this study, we validated analyses of the Ekman model published by Lilly and Brown who identified the indirect inflection-point or f_V-mechanism of instability, and by Leibovich and Lele who identified the direct f_H-mechanism of instability. We also use a zero-hypothesis, which states that there is no significant effect of the Coriolis force on the turbulence structure of the EBL. Our study unambiguously reveals that the direct f_H-mechanism of instability is the dominant instability mechanism structuring the EBL turbulence. This mechanism (Leibovich and Lele, 1985) attributes the large scale structure of the EBL to the direct action of the horizontal component of the Coriolis force, which pumps energy into the vortex rolls when the mean flow velocity vector is aligned with the Coriolis force vector. As the Coriolis force does not change the total flow energy in domain, the large effect of this alignment is caused by the energy redistribution across the turbulence spectrum. The increase of the TKE on the largest EBL scales is followed by the corresponding decrease in the effective eddy viscosity so that the actual turbulent stress (measured by the friction velocity or the geostrophic drag coefficient) changes less significantly. In these simulations, the total kinetic energy of the flow in the domain still varies from run to run. This is due to the turbulence closure algorithm, which calculates the local effective eddy viscosity on the basis of the TKE of the smallest resolved scale turbulence. It is presently unclear whether these variations in the total kinetic energy in the domain are a numerical artifact or there is some physics involved. One reasonable possibility would be to involve the spectral re-distribution of energy that interferes with the pressure tensor (return-to-isotropy hypothesis; Launder et al., 1975), which makes the EBL with smaller scale turbulence more dissipative.

Without viscous effects, the f_H-mechanism of instability is just the consequence of flow angular momentum conservation in the rotated frame of reference. The viscous effects give raise non-trivial features of self-organization in the form of the longitudinal rolls and the TKE concentration at the largest turbulence

scales. The obtained characteristics of the rolls remind the distinct features of the inactive turbulence introduced by Townsend (1961).

The largest differences in the EBL structure were found in low latitudes where the f_H-mechanism is the strongest. Here, the turbulence in the EBL driven by easterlies is organized in pronounced regular rolls, which comprise the entire EBL. By contrast, the turbulence in the EBL driven with westerlies remains unorganized and small scale. The polar EBL, where the f_H-mechanism is absent, does not show any structural differences with respect to the direction of the geostrophic wind. Nevertheless, somewhat weaker rolls are also recognizable in the polar EBL. The structures in the polar EBL are less energetic and less regular than in the low-latitude EBL. This feature suggests that the f_V-mechanism of instability may be also acting in the EBL.

The recent work by Fricke (2011) gives a possibility to compare the results of this study with the EBL simulations in a fully three-dimensional but smaller domain. Although the complete statistical analysis has not been presented by Fricke, the available results agree qualitatively and quantitatively with the results of this study. In particular, the leading role of the f_H-mechanism of instability in low latitudes has been confirmed. Moreover, the three-dimensional simulations confirmed that the large scale turbulent structures are shaped as counter-rotating rolls roughly aligned with the geostrophic wind.

Acknowledgements – The research leading to these results has received funding from: the European Union's Seventh Framework Programme FP/2007-2011 under grant agreement **№** 212520; the Norwegian Research Council basic research programme project PBL-feedback 191516/V30; the Norwegian Research Council project RECON 200610/S30; the European Research Council Advanced Grant, FP7-IDEAS, 227915; and by a grant from the Government of the Russian Federation under contract **№** 11.G34.31.0048. The author acknowledges fruitful discussions with and support from Dr. A. Glazunov (Institute for Numerical Mathematics, Moscow, Russia) and Mr. J. Fricke (Institute for Meteorology and Climatology at Leibniz University in Hannover, Germany). The special gratitude should be given to the Bjerknes Centre for Climate Research (Bergen, Norway) and the Norwegian programme NOTUR for the generous support and funding over many years.

References

Atkinson, B. W. and Zhang, J. W. (1996): Mesoscale shallow convection in the atmosphere, *Rev. Geophys.*, **34**, 403–431.

Barthlott, Ch., Drobinski, Ph., Fesquet, C., Dubos, Th. and Pietras, Ch. (2007): Long-term study of coherent structures in the atmospheric surface layer, *Bound.-Lay. Meteorol.*, **125**, 1–24.

Beare, R. J., MacVean, M. K., Holtslag, A. A. M., Cuxart, J., Esau, I., Golaz, J.-C., Jimenez, M. A., Khairoutdinov, M., Kosovic, B., Lewellen, D., Lund, T. S., Lundquist, J. K., McCabe, A., Moene, A. F., Noh, Y., Raasch, S. and Sullivan, P. P. (2006): An intercomparison of large-eddy simulations of the stable boundary layer, *Bound.-Lay. Meteorol.*, **118**(2), 247–272.

Bradshaw, P. (1969): The analogy between streamline curvature and buoyancy in turbulent shear flow, *J. Fluid Mech.*, **36,** 177–191.

Brown, R. A. (1970): A secondary flow model for the planetary boundary layer, *J. Atmos. Sci*., **27**, 742–757.

Caldwell, D. R., van Atta, C. W. and Helland, K. N. (1972): A laboratory study of the turbulent Ekman layer, *Geophys. Fluid Dyn*., **3**, 125–160.

Chereshkin, T. K. (1995): Direct evidence for an Ekman balance in the Californian Current, *J. Geophys. Res.*, **100**, 18261–18269.

Coleman, G. N., Ferziger, J. H. and Spalart, P. R. (1990): A numerical study of the turbulent Ekman layer, *J. Fluid Mech*., **213**, 313–348.

Drobinski, P. and Foster, R. C. (2003): On the origin of near-surface streaks in the neutrally stratified planetary boundary layer, *Bound.-Lay. Meteorol.*, **108**, 247–256.

Ekman, V. W. (1905): On the influence of the Earth's rotation on ocean currents, *Ark. Mat. Astron. Fys*., **2**, 1–53.

Esau, I. (2003): Coriolis effect on coherent structures in planetary boundary layers, *J. Turbul.*, **4**, 017.

Esau, I. (2004): Simulation of Ekman boundary layers by large eddy model with dynamic mixed subfilter closure, *Environ. Fluid Mech.*, **4**, 273–303.

Esau, I. and Zilitinkevich, S. S. (2006): Universal dependences between turbulent and mean flow parameters in stably and neutrally stratified planetary boundary layers, *Nonlinear Proc. Geophys.*, **13**, 122–144.

Etling, D. and Brown, R. A. (1993): Roll vortices in the planetary boundary layer: A review, *Bound.-Lay. Meteorol.*, **65**, 215–248.

Foster, R. C., Vianey, F., Drobinski, P. and Carlotti, P. (2006): Near-surface coherent structures and the vertical momentum flux in a large-eddy simulation of the neutrally-stratified boundary layer, *Bound.-Lay. Meteorol.*, **120**(2), 229–255.

Fricke, J. (2011): Coriolis instabilities in coupled atmosphere-ocean large-eddy simulations, M.Sc. Thesis, Institute of Meteorolology and Climatolology, Leibniz University, Hannover, Germany, 87 pp.

Haack, T. and Shirer, H. N. (1992): Mixed convective/dynamic roll vortices and their effects on initial wind and temperature profiles, *J. Atmos. Sci.*, **49**, 1181–1201.

Haeusser, T. M. and Leibovich, S. (2003): Pattern formation in the marginally unstable Ekman layer, *J. Fluid Mech*., **479**, 125–144.

Howroyd, G. C. and Slawson, P. R. (1975): The characteristics of a laboratory produced turbulent Ekman layer, *Bound.-Lay. Meteorol.*, **8**, 201–219.

Huang, J., Cassiani, M. and Albertson, J. D. (2009): Analysis of coherent structures within the atmospheric boundary layer, *Bound.-Lay. Meteorol.*, **131**, 147–171.

Gerkema, T., Zimmerman, J. T. F., Maas, L. R. M. and van Haren, H. (2008): Geophysical and astrophysical fluid dynamics beyond the traditional approximation, *Rev. Geophys*., **46**, RG2004, DOI: 10.1029/2006RG000220.

Grimsdell, A. W. and Angevine, W. M. (2002): Observations of the afternoon transition of the convective boundary layer, *J. Appl. Meteorol*., **41**(1), 3–11.

Grisogono, B. (1995): A generalized Ekman layer profile with gradually varying eddy diffusivities, *Q. J. Roy. Meteorol. Soc.,* **121**, 445-453.

Johnston, J. (1998): Effects of system rotation on turbulence structure: A review relevant to turbomachinery flows, *Int. J. Rotating Machinery*, **4**(2), 97–112, DOI: 10.1155/S1023621X98000098.

Kumar, V., Kleissl, J., Meneveau C. and Parlange, M. B. (2006): Large-eddy simulation of a diurnal cycle of the atmospheric boundary layer: Atmospheric stability and scaling issues, *Water Resour. Res*., **42**, W06D09, DOI: 10.1029/2005WR004651.

Larsen, S. E., Olesen, H. R. and Højstrup, J. (1985): Parameterization of the low frequency part of spectra of horizontal velocity components in the stable surface boundary layer, in *Turbulence and Diffusion in Stable Environments,* edited by Hunt, J. C. R., Clarendon Press, Oxford, UK, 181–204.

Launder, B. E., Reece, G. J. and Rodi, W. (1975): Progress in the development of a Reynolds-stress turbulent closure, *J. Fluid Mech.*, 68(3), 537–566.

Leibovich, S. and Lele, S. K. (1985): The influence of the horizontal component of the Earth's angular velocity on the instability of the Ekman layer, *J. Fluid Mech.*, 150, 41–87.

Lilly, D. (1966): On the instability of Ekman boundary flow, *J. Atmos. Sci.*, 23, 481–494.

Lin, C.-L., McWilliams, J., Moeng, C.-H. and Sullivan, P. (1996): Coherent structures and dynamics in a neutrally stratified planetary boundary layer flow, *Phys. Fluids*, **8,** 2626–2639.

Lin, C.-L., Moeng, C.-H., Sullivan, P. P. and McWilliams, J. C. (1997): The effect of surface roughness on flow structures in a neutrally stratified planetary boundary layer flow, *Phys. Fluids*, **9**, 3235, DOI: 10.1063/1.869439.

Mason, P. J. and Sykes, R. I. (1980): A two-dimensional numerical study of horizontal roll vortices in the neutral atmospheric boundary-layer, *Q. J. Roy. Meteorol. Soc.*, **106**, 351–366.

Miles, J. W. (1994): Analytical solutions for the Ekman layer, *Bound.-Lay. Meteorol.*, **67**, 1–10.

Mininni, P. D., Alexakis, A. and Pouquet, A. (2009): Scale interactions and scaling laws in rotating flows at moderate Rossby numbers and large Reynolds numbers, *Phys. Fluids*, **21**, 015108, DOI: 10.1063/1.3064122.

Mironov, D. V., Gryanik, V. M., Moeng, C.-H., Olbers, D. J. and Warncke, T. H (2000): Vertical turbulence structure and second-moment budgets in convection with rotation: A large-eddy simulation study, *Q. J. Roy. Meteor. Soc.*, **126**, 477–515.

Miyashita, K., Iwamoto, K. and Kawamura, H. (2006): Direct numerical simulation of the neutrally stratified turbulent Ekman boundary layer, *J. Earth Simulator*, **6**, 3–15.

Ponomarev, V. M., Chkhetiani, O. G. and Shestakova, L. V. (2007): Nonlinear dynamics of large-scale vortex structures in a turbulent Ekman layer, *Fluid Dyn.*, **42**(4), 571–580.

Price, J. F., Weller, R. A. and Schudlich, R. R. (1987): Wind-driven ocean currents and Ekman transport, *Science*, **238**, 1534–1538.

Rossby, C. G. and Montgomery, R. B. (1935): The layers of frictional influence in wind and ocean currents, *Pap. Phys. Oceanogr. Meteorol.*, **3**, 1–101.

Salhi, A. and Cambon, C. (1997): An analysis of rotating shear flow using linear theory and DNS and LES results, *J. Fluid Mech.*, **347**, 171–195.

Savtchenko, A. (1999): Effect of large eddies on atmospheric surface layer turbulence and the underlying wave field, *J. Geophys. Res.*, **104**, 3149–3157.

Spalart, P. R., Coleman, G. N. and Johnstone, R. (2008): Direct numerical simulation of the Ekman layer: a step in Reynolds number, and cautious support for a log law with a shifted origin, *Phys. Fluids*, **20**(10), DOI: 10.1063/1.3005858.

Schoppa, W. and Hussain, F. (1998): Numerical study of near-wall coherent structures and their control in turbulent boundary layers, in *16th Int. Conf. on Numerical Methods in Fluid Dynamics, Lect. Notes Phys.*, **515**, 103–116.

Soloviev, A. (1990): Coherent structures at the ocean surface in convectively unstable conditions, *Nature*, **346**, 157-160.

Sullivan, P. P., Horst, Th. W., Lenschow, D. H., Moeng, C.-H. and Weil, J. C. (2003): Structure of subfilter-scale fluxes in the atmospheric surface layer with application to large-eddy simulation modeling, *J. Fluid Mech.*, **482**, 101–139.

Tan, Z.-M. (2001): An approximate analytical solution for the baroclinic and variable eddy diffusivity semi-geostrophic Ekman boundary layer, *Bound.-Lay. Meteorol.*, **98**, 361–385.

Tennekes, H. (1973): A model of the dynamics of the inversion above a convective boundary layer, *J. Atmos. Sci.*, **30**, 558–567.

Townsend, A. A. (1961): Equilibrium layers and wall turbulence, *J. Fluid Mech.*, **11**, 97–120.

Tritton, D. J. (1992): Stabilization and destabilization of turbulent shear flow in a rotating fluid, *J. Fluid Mech.*, **241,** 503–523.

Vreman, B., Geurts, B. and Kuerten, H. (1997): Large-eddy simulation of the turbulent mixing layer, *J. Fluid Mech.*, **339**, 357–390.

Wijffels, S., Firing, E. and Bryden, H. L. (1994): Direct observations of the Ekman balance at 10° N in the Pacific, *J. Phys. Oceanogr.*, **24**, 1666–1679.

Zhang, G., Xu, X. and Wang, J. (2003): A dynamic study of Ekman characteristics by using 1998 SCSMEX and TIPEX boundary layer data, *Adv. Atmos. Sci.*, **20**(3), 349–356.

Zeytounian, R. Kh. (2003): On the foundation of the Boussinesq approximation applicable to atmospheric motions, *Izv. Atmos. Ocean. Phys.*, **39**(Suppl. 1), S1–S14.

Zikanov, O., Slinn, D. N. and Dhanak, M. R. (2003): Large-eddy simulations of the wind-induced turbulent Ekman layer, *J. Fluid Mech.*, **495**, 343–368.

Zilitinkevich, S. S. and Esau, I. (2005): Resistance and heat transfer laws for stable and neutral planetary boundary layers: Old theory, advanced and re-evaluated, *Q. J. Roy. Meteorol. Soc.*, **131**, 1863-1892, DOI: 10.1256/qj.04.143.

Zilitinkevich, S., Esau, I. and Baklanov, A. (2007): Further comments on the equilibrium height of neutral and stable planetary boundary layers, *Q. J. Roy. Meteorol. Soc.*, **133**, 265–271.

Appendix. Correlation length scale analysis of simulations

The apparent size of the vortex pair in the A180U5L5 run is about 6 km in Fig. 9. The cross-flow size of the domain is 144 km. This size is sufficient to accommodate 25 pairs of the counter-rotating vortices. Thus, the simulations provide sufficient material for objective statistical analysis of the large scale turbulence in the EBL. This study is focused on the correlation analysis of the vertical momentum flux. We describe the method using the run A180U5L5 where the turbulent eddies were the largest.

Fig. A1 shows one cross-flow sub-section (36 km) of the streamwise component of the vertical momentum flux $\tau_{uw}(x,y,z)$ averaged over the last hour of simulations. The run dimension in the cross-flow direction is N_y = 4096. Therefore, $N_y/2-1$ auto-correlation coefficients $R_{uw}(x,r,z) = corr\,(\tau_{uw}(x,y,z), \tau_{uw}(x,y+r,z))$, will be calculated. Here, r is the relative separation of two points in the cross-flow direction. These coefficients will slightly differ for each of the cross-flow section along the streamwise direction. These variations are used to compute standard deviations of the coefficients, and therefore, to estimate robustness of the analysis. Fig. A2 shows the calculated coefficients $R_{uw}(\delta_y,z)$ at 4 model levels corresponding to 0.1, 0.2, 0.5 and 1.0 of the estimated EBL thickness, h. The auto-

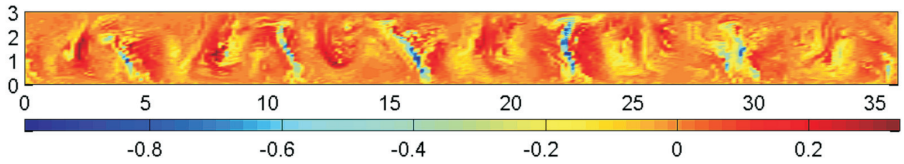

Figure A1. A cross-flow section of the streamwise component of the vertical kinematic momentum flux τ^x_{uw} [m^2 s^{-2}] (colour shading) averaged in the streamwise direction in the run A180U5L5. The distances on the *y*-axis (the horizontal cross-flow axis) and the *z*-axis (the vertical axis) are given in km. The negative values correspond to the downward momentum transport.

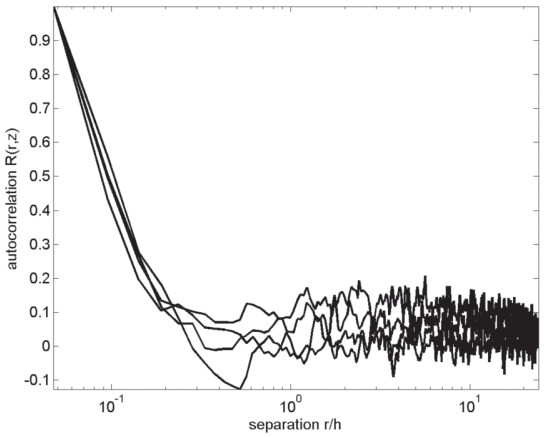

Figure A2. The auto-correlation coefficients of the streamwise vertical momentum flux at the model levels corresponding to 0.1, 0.2, 0.5 and 1.0 EBL thickness, h. The separation r gives the shift of the auto-correlation in the cross-flow direction.

correlation coefficient decay quickly from unity to some negative value, which signals the change of sign of the momentum flux.

The correlation length scale, λ, is defined as the separation r where the minimum negative auto-correlation has been reached. In the case of well developed turbulent large-scale structures, like in the EBL core sub-layer in Fig. 9 and in Fig. A1, the minimum is well-defined. But in the case of irregular structures, λ could be ill-defined. To reduce ambiguity of the scale definition, this study uses averaging of the defined length scales in the streamwise direction and across 4 adjacent model levels.

SAŽETAK

Turbulentne strukture većih dimenzija u Ekmanovom graničnom sloju

Igor Esau

Ekmanov granični sloj (EGS) je nestratificirani turbulentni sloj u rotirajućem fluidu. EGS se učestalo opaža i u atmosferi i u oceanu. Sastoji se od dva podsloja: od površinskog, u kojem dominira dobro razvijena turbulencija male skale, i središnjeg, u kojem dominira samoorganizirana turbulencija veće skale. Ova studija prikazuje samoorganiziranu turbulenciju veće skale u EGS-u, koja je simulirana modelom velikihx vrtloga (LES) nazvanim LESNIC. Kako bi se odredio statistički značajan broj najvećih samoorganiziranih vrtloga, simulacije su rađene na velikoj domeni (144 km u smjeru okomitom na strujanje, što približno odgovara pedeseterostrukoj debljini EGS-a). Analiza je pokazala da zemljopisna širina LES domene i, neočekivano, smjer forsirajućeg geostrofičkog vjetra

kontroliraju samoorganiziranost, skale turbulencije, razvoj i kvazistacionarno stanje usrednjenih vertikalnih profila u EGS-u. LES rezultati su pokazali destabilizaciju EGS turbulencije i njene srednje strukture s horizontalnom komponentom Coriolisove sile. Vizualizacija EGS-a je otkrila postojanja skoro pravilnih turbulentnih struktura velike skale, koje su se u slučaju promjene geostrofičkog vjetra od istočnog u zapadni, sastojale od vrloga sa suprotnom rotacijom. Odgovarajuće strukture nisu bile prisutne u EGS-u ukoliko je vjetar mijenjan u suprotnom smjeru (od zapada prema istoku). Ovi rezultati u konačnici rješavaju dugo prisutnu polemiku između Leibovich-Leleovog i Lilly-Brownovog mehanizma nestabilnosti, koji djeluju u EGS-u. LES simulacije pokazuju da Lilly-Brownov mehanizam, koji uključuje vertikalnu komponentu Coriolisove sile, vrijedi u polarnom EGS-u, gdje je njegov utjecaj ipak malen. Leibovich-Leleov mehanizam, koji uključuje horizontalnu komponentu Coriolisove sile, djeluje na nižim zemljopisnim širinama, gdje u potpunosti mijenja turbulentnu strukturu EGS.

Ključne riječi: atmosferski granični sloj, simulacije velikih vrtloga, Ekmanov granični sloj, samoorganizirana turbulencija

Corresponding author's address: Igor Esau, Thormohlensgt. 47, 5006 Bergen, Norway, e-mail: igor.ezau@nersc.no